Advances in Nano Research, *Vol. 16, No. 1 (2024) 53-69*
https://doi.org/10.12989/anr.2024.16.1.053

Characterization of nano-structure pyrolytic char for smart and sustainable nanomaterials

N. K. Karthikeyan[a] and S. Elavenil*

School of Civil Engineering, Vellore Institute of Technology, Chennai-campus, Vandalur – kelambakkam road, Chennai 600127, India

(*Received August 18, 2023, Revised October 17, 2023, Accepted October 19, 2023*)

Abstract. Advancements in the technology of building materials has led to diverse applications of nanomaterials with the aim to monitor concrete structures. While there are myriad instances of the use of nanoparticles in building materials, the production of smart nano cement-composites is often expensive. Thereupon, this research aims to discover a sustainable nanomaterial from tyre waste using the pyrolysis process as part of the green manufacturing circle. Here, Nano Structure Tyre-Char (NSTC) is introduced as a zero-dimension carbon-based nanoparticle. The NSTC particles were characterized using various standard characterization techniques. Several salient results for the NSTC particles were obtained using microscopic and spectroscopic techniques. The size of the particles as well as that of the agglomerates were reduced significantly using the milling process and the results were validated through a scanning electron microscope. The crystallite size and crystallinity were found to be ~35nm and 10.42%, respectively. The direct bandgap value of 5.93eV and good optical conductivity at 786 nm were obtained from the ultra violet visible spectroscopy measurements. The thermal analysis reveals the presence of a substantial amount of carbon, the rate of maximum weight loss, and the two stages of phase transformation. The FT-Raman confirms the presence of carboxyl groups and a ID/IG ratio of 0.83. Water contact angle around 140º on the surface implies the highly hydrophobic nature of the material and its low surface energy. This characteristic process assists to obtain a sustainable nanomaterial from waste tyres, contributing to the development of a smart building material.

Keywords: characterization; microscopic; spectroscopic; sustainable nanomaterial; waste tyre

1. Introduction

Recent years have witnessed the use of nanomaterials in the construction industry to improve the integrity of concrete structures. Despite their merits, the application of nanomaterials in practical applications suffers serious drawbacks such as uneconomical, increased complications, and hazardous nature of the nanoparticles due to their reduced particle size, etc., which has prompted the idea of introducing sustainable nanomaterials. The development in nanotechnology has also led to the idea of using nanoparticle as building material to produce smart-sensing cement matrix Kanagasundaram and Solaiyan (2023). Extensive researches have been carried out for a decade in exploring several carbon nanomaterials and reinforcing them into cement matrix. However, conflicting results in fabricating nanocomposites have been reported. The search for sustainable nanomaterials instead of commercial nanomaterials has been on the rise. In this context, utilizing waste tyres which make up for almost 2-3% of the total global waste will be an ideal choice to produce sustainable nanomaterials.

Globally, tyres are produced in large volume and India represents the fourth largest market size by producing about 188.9 million units in 2022 IMARC (2022). Inevitably, around 100 million of end-of-life tyres are generated in India every year according to "Material Recycling Association of India (MRAI). Tyres are primarily manufactured using rubber, carbon black, metal, textile, zinc oxide, sulphur, and other additives (Banasiak *et al*. 2019). As the life of a tyre ends, it is accumulated in stock piles and land fill causing fire hazard and other significant problems (leaching toxic chemical) to the environment. The continuous accumulation of waste tyres has become a challenging issue that compounds the recycling task. Therefore, researchers across the world have collectively proposed the idea of recovering waste tyre to be utilized in civil engineering applications as a sustainable construction material (Moasas *et al*. 2022). These waste tyre resources are potentially embedded with high carbon content that is valuable for several advanced developments (Abbas-Abadi *et al*. 2022). Consequently, a sustainable method without waste by-products is indispensable to recycle end-of-life tyres for recovering sustainable nano carbon resources.

Among the several methods in use, pyrolysis offers a feasible way to convert the end-of-life tyres into char, liquid, and gases and thus to extract sustainable nano carbon. Pyrolysis is one of the green and renewable alternatives compared to land filling, re-processing, and incineration. The quality of the products (char, oil, and gas) obtained through pyrolysis treatment is crucially dependent on temperature, time, atmosphere, pressure, and the type of furnace used. The schematic illustration of the setup for pyrolysis treatment is depicted in Fig. 1. Pyrolysis oil is mixture of hydrocarbons further refined to produce fuel

*Corresponding author, Professor
E-mail: elavenil.s@vit.ac.in
[a] Research Associate,
E-mail: karthikeyan.nk2020@vitstudent.ac.in

ISSN: 2287-237X (Print), 2287-2388 (Online)

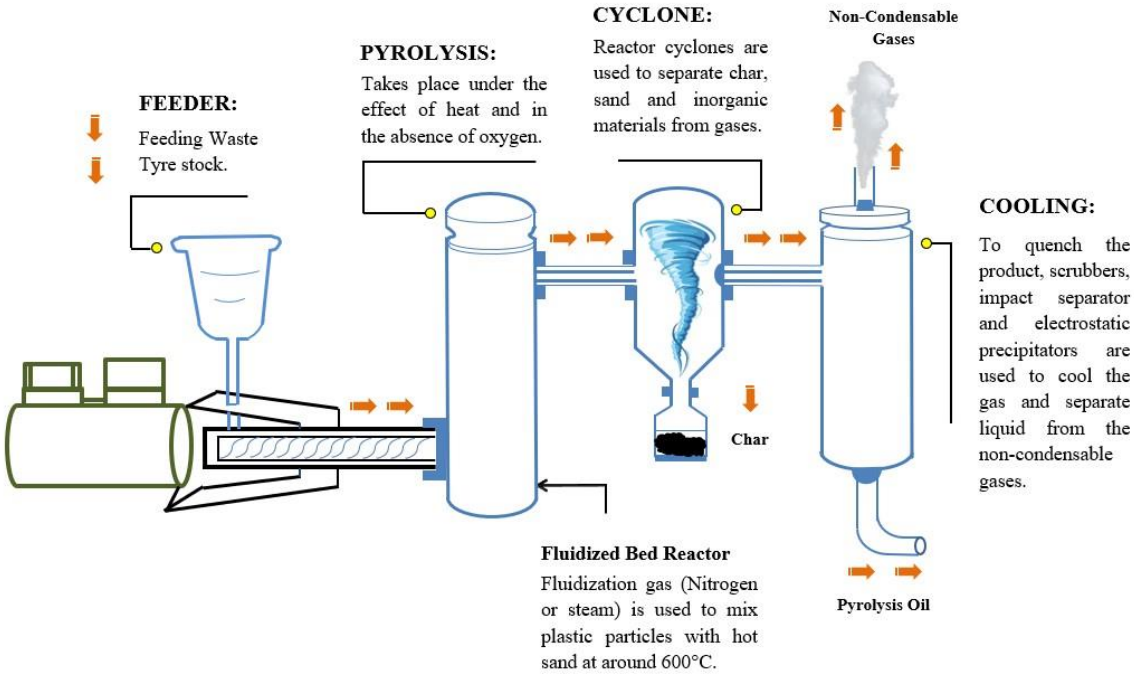

Fig. 1 Schematic illustration of recycling waste tyres by fast pyrolysis treatment

products. Whereas, collected gases serve as precursor to produce fuels and chemicals. Moreover, other products such as steel wire, non-condensable gas and condensable vapors are collected from pyrolysis and used for recycling and energy recovery process, respectively. In general, end-of-life tyres are heated between 400-600°C in the absence of oxygen. At temperatures between 500-550°C, the process yields tyre char (solid product) (Parthasarathy *et al*. 2016, Maroufi *et al*. 2017, Goksal 2022, Wang *et al*. 2023). The mass balance of tire pyrolysis process for char, oil, gas, and steel wire are 37.45%, 39.62%, 13.32%, and 9.95%, respectively. The potentially valuable tyre char/NSTC particles produced by pyrolysis treatment that contains rich carbon black (80-90%) is the theme of this study. The highly value-added applications of tyre char included gasification, adsorbent, catalyst, batteries, and reinforcing agents for rubber formulations. Moreover, pyrolysis carbon black from waste tire having unique properties is processed for various practical application such as to produce water-based inkjet printing ink Wu and Liao (2021), high value in natural rubber composites (Ma *et al*. 2022), electrode material for supercapacitors (Chen *et al*. 2021), and developing thermal insulation materials (Zhao *et al*. 2023). Additionally, these tyre carbon black potentially used for environmental remediation like filtering or cleaning waste water efficiently (Trubetskaya *et al*. 2019). The size, structure, and other physico-chemical characteristics of tyre char with carbon origin have attracted research interest in the construction material, over the years. Tyre char is risen as an affordable source of nano carbon particle with potential benefits including high surface area to volume ratio, favourable electrical conductivity, and excellent mechanical resilience (Maroufi *et al*. 2017, Martínez *et al*. 2019, Gao *et al*. 2022).

Several researchers have reported the use of crumb and shredded tyres as construction material to modify the behaviour of concrete and enhance their properties (Mohajerani *et al*. 2020). Besides, the characteristics features of NSTC particle/tyre char have increased the research interest for their utilization as concrete additives. Paul *et al*. characterized pyrolytic carbon black/tyre char using several techniques and observed that it exhibited similar features as that of commercially available carbon black. Therefore, he proposed pyrolytic carbon black as an alternative reinforcing filler to commercial carbon black (Paul *et al*. 2023). Further, Mahmood *et al*. and Khalid *et al*. experimentally proved that the use of pyrolytic carbonized waste tyre as a nano inert (1%) in cementitious composites significantly improved their compressive strength (43.1%), fracture toughness, electromagnetic interference shielding, while also reducing the porosity (Mahmood *et al*. 2020, Khalid *et al*. 2022). Moreover, Sardar *et al*. developed high-strength fire resistant concrete by incorporating pyrolytic tyre char as an additive. The authors proved that tyre char incorporated concrete has the ability to reduce spalling even at temperatures of 800°C. Further, the 1% of tyre char addition was optimized for better residual performance of the mechanical properties at elevated temperatures (Sardar *et al*. 2022).

Tyre char is also used to develop high absorption capacity Phase Change Material (PCM) for the construction industry. Ryms *et al*. conducted different studies on the sustainable application of pyrolytic carbon as a PCM carrier in cementitious composites. The addition of modified pyrolytic carbon to cement mortar was found to enhance the high energy saving capacity, heat accumulation, and heat release at different phases of transition in the construction. He also demonstrated that pyrolytic carbon based PCM

carrier in cement matrix enhances the energy efficiency and thermal comfort of the building for energy-saving construction (Ryms *et al*. 2020, 2022). In addition to construction materials, tyre char is also employed in another relevant construction sector to produce bitumen as a binder material for roads. Reinforcing tyre char into bitumen facilitates their multifunctional application by improving their rheological properties (Chaala *et al*. 1996, Li *et al*. 2018), ageing resistance (Feng *et al*. 2016), temperature resistance (Feng *et al*. 2021), and electrothermal properties (Wang *et al*. 2019).

Firstly, although NSTC particles have been employed as additives in concrete and bitumen, the role of NSTC particle as a sustainable nano carbon in cement composites is not yet reported. Secondly, none of the reported research works has emphasized the complete characterization of NSTC particles. Despite the several researches carried out on using tyre char as a supplementary material, there is lack in examining the nano properties of NSTC particle such as bandgap, thermal, hydrophobic, and bonding properties. The present novelty of the study is to determine and standardize the nano properties of NSTC particle using different nano characterization techniques before incorporating them into cement matrix. The physico-chemical characterization of NSTC particles using different techniques is performed and demonstrating the ability of these particles to cope up with the cementitious nature for self-sensing property will be the key gap of knowledge. Certainly, from the results obtained, NSTC particle is predicted to perform as a sustainable nanomaterial in comparison to commercially available nanomaterials.

2. Experimental

2.1 Material

NSTC particles are carbon residues obtained during the pyrolysis treatment of end-of-life-tyres at temperatures ranging from 500-550 ºC. This high pyrolysis temperature can facilitate the enhanced decomposition and more valuable product with less residue. Since they are obtained from waste tyres, they represent a potential source of carbon that can be used as a cost-effective nanomaterial for several applications. The NSTC particles used for the present study were acquired from GS Pyro Enterprise Pvt. Ltd., India, and is shown in Fig. 2. The physical properties of the NSTC particles were determined using standard laboratory tests. The oxide compositions of NSTC particle obtained by X-Ray Fluorescence (XRF) spectroscopy are summarized in Table 1. The oil absorption (DBP) and pH value were determined according to IS 33 (1992) and IS 877 (1989) standards, respectively. The DBP results revealed class I carbon and expressed in 'ml' of oil in 100g using (100V/m). The surface area, total pore volume, and mean pore diameter were determined using the Brunauer-Emmett-Teller (BET) model, while the pore size distribution was determined using Barrett Joyner Halenda (BJH) model. The percentage of loss on ignition was determined according to IS1612:1976 and was found to be 81.5%.

Fig. 2 Photograph of the NSTC particles

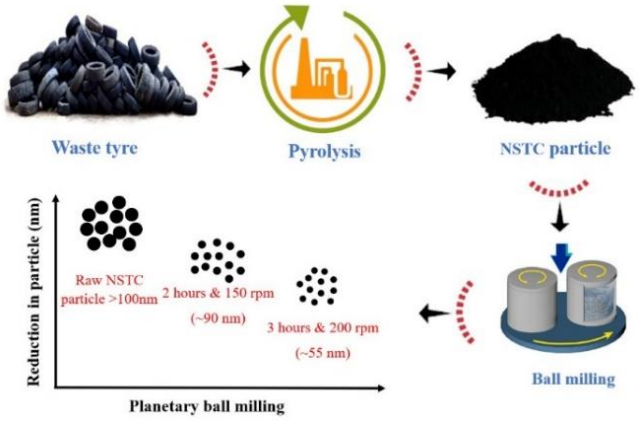

Fig. 3 Processing method of NSTC particle

2.2 Chacracterization techniques

The solid char generated after the pyrolysis of waste tyre constitutes the NSTC particle, which is the predominant product and is similar to carbon black. Further, NSTC particles was grinded to reduce the size of the material below 100 nm, the processing of material is depicted in the Fig. 3. Owing to its high carbon content, it is essential to understand the properties of NSTC particles such as surface morphology, crystallinity, pore size distribution, element surface, thermal and optoelectronic properties. Hence, NSTC particles are subjected to various nano characterization techniques to enable their utility as a sustainable nano-material in cement matrix as well as for distinct applications. By considering this fact, different microscopic and spectroscopic techniques as shown in Fig. 4 were employed. The microscopic techniques such as Scanning Electron Microscope (SEM), High-Resolution Scanning Electron Microscope (HR-SEM) with EDX and mapping, and spectroscopic techniques such as X-ray powder Diffraction (XRD), Ultra Violet - Visible (UV-Vis) spectro-scopy, and Fourier Transform - Raman (FTR) spectroscopy was employed. Furthermore, Thermal Gravimetric Analysis (TGA), Derivative Thermogravimetric (DTG) and Differential Scanning Calorimetry (DSC) were employed to characterize the NSTC particles. Besides, Water Contact Angle (WCA) on the given surface was also determined. Meanwhile, Carbon, Hydrogen, Nitrogen, Sulphur, Oxygen (CHNSO) content determination and ball milling process were also employed to obtain a complete characterization of the NSTC particles. The characterization techniques employed

Table 1 Physical properties and chemical composition of the NSTC particles obtained by XRF

NSTC particle			
Physical properties		XRF composition (%)	
Appearance	Black	SiO_2	7.01
Average Particle size	130nm	TiO_2	0.14
DBP* Oil absorption	110ml/100g	Al_2O_3	0.55
Fixed Carbon	> 80%	MnO	0.00559
Specific gravity	1.89	Fe_2O_3	0.91
Surface area ($a_{s, BET}$)	29.5 m^2/g	CaO	0.99
Total pore volume ($p/p_0 = 0.902$)	0.051cm^3/g	MgO	0.16
Mean pore diameter	7.6781nm	Na_2O	0.58
Pore size distribution ($r_{p, peak}$ area)	1.22nm	K_2O	0.11
pH value	6.3	P_2O_5	0.073
Porosity (%)	2.22	LOI*	81.5

*DBP : Dibutyl Phthalate, LOI : Loss on Ignition

Table 2 List of physicochemical characterization techniques carried out on the NSTC particles

Properties of NSTC particle	Characterization techniques
Carbon content and Molecular formula	CHNSO Analysis
Particle size, shape and aggregation state	Scanning Electron Microscope (SEM)
Elemental surface analysis	High Resolution - Scanning Electron Microscope (HR-SEM) with Energy Dispersive X-ray spectroscopy (EDX)
Crystallite size and polymorph crystallinity	X-ray powder Diffraction (XRD)
Composition	X-ray Fluorescence spectroscopy (XRF)
Bonding Structure	Fourier Transform - Raman spectroscopy (FT-Raman)
Thermal properties	Thermal Gravimetric Analysis (TGA) Derivative Thermogravimetric (DTG) Differential Scanning Calorimetry (DSC)
Optoelectronic properties	Ultra Violet - Visible spectroscopy (UV-Vis)
Hydrophobicity and Surface energy	Water Contact Angle (WCA)

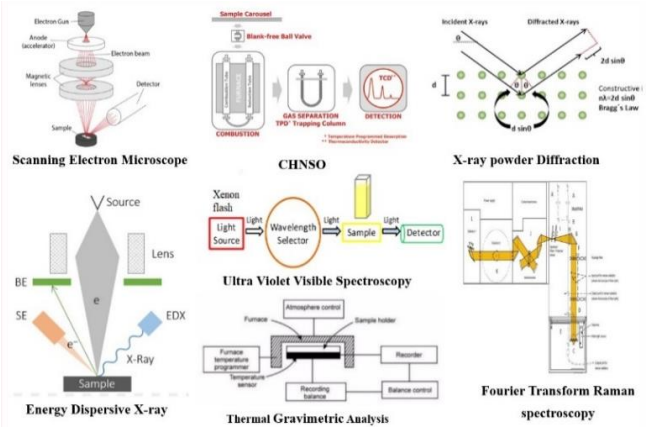

Fig. 4 Various microscopic and spectroscopic techniques

to determine the various parameters of the NSTC particle are tabulated in Table 2 and the results of the characterization are discussed in detail in the subsequent sections.

2.2.1 SEM and ball milling

In order to achieve the desired particle size and homogeneity of the NSTC particles, the ball milling technique was adopted using planetary ball mill (VB ceramics) having 10 mm Zirconia balls, single grinding station with less than 10 mm feed size and 250 ml jar size. This desired particle size was achieved by monitoring and controlling the milling parameters such as the rotation speed, milling time, and ball to powder ratio. SEM was employed for the microstructural analysis on the sample before and after the ball milling process using TESCAN VEGA3 instrument with an accelerated voltage of 30 kV. The samples were coated with gold and Secondary Electron (SE) imaging was performed. SEM analysis provided information about the reduction in particle size and the size distribution, morphology, and aggregation state of the particles, both at the micro and nano-scales.

2.2.2 CHNSO element analyzer

Further characterization on the NSTC particles were carried out to determine the carbon, hydrogen, nitrogen, sulphur, and oxygen content using a CHNSO element analyzer. The vario MICRO cube elemental analyzer (5mgChem90s method) having an advanced purge and trap technology that is capable of determining C:N elemental ratio of up to 5000:1 was utilized. The tests were performed according to the standards at a combustion tube temperature

of 1150 ºC, reduction tube temperature of 850 ºC with helium gas used as a carrier at a flow rate 213-223 ml/min.

Furthermore, the molecular formula/empirical formula and molecular mass of NSTC particles were formulated.

2.2.3 XRD

XRD was employed to characterize the polymorph crystallinity, crystallite size, and crystallographic structure of the NSTC particles. The diffractogram of the NSTC particles was obtained using a RIGAKU Smartlab 3kW (200V, 50/60 Hz, 3Φ 30A) instrument. The analysis was carried out in the fast scan mode with a ramp of 0.02º (2θ) using CuKά radiation (λ = 1.54 Å) operated at an accelerated voltage of 40 kV and current of 30 mA. The pattern was recorded by continuous '2θ' diffraction scan ranging from 5º to 80º at a scan speed of 5º/min. The phase identification and its quantification were performed using X'pert high score plus software while the crystallinity (%) were ascertained using the Origin-Pro software. The average crystallite size of the NSTC particles were determined using the Debye-Scherrer equation.

2.2.4 HR-SEM / EDX / Mapping

HR-SEM was employed to identify the surface texture, microstructure, and morphology of the NSTC particles. In addition, EDX analysis provided information on the weight and atomic composition of the different elements in percentage. Thus, using HR-SEM via EDX, the different elements present in the NSTC particles and their composition were estimated. Additionally, mapping was performed to illustrate the distribution of various elements in the NSTC sample. The versatile QUANTA FEG 200F instrument was used for HR-SEM/EDX/Mapping, wherein the experiments were carried out at high vacuum acceleration voltage of 20 kV using SE imaging mode.

2.2.5 UV-VIS spectroscopy

The optical band gap and optical conductivity are the crucial parameters that determine the conductivity and the electronic state, respectively of a conductive material. DRA Evolution 300 instrument that offers a direct and convenient way to study the band gap energy and optical conductivity was used to obtain UV-VIS spectrum of NSTC particles. The bandgap of the material was plotted for direct and indirect allowed transition relation as a function of the incident photon energy ($h\nu$) using Tauc's method. UV-VIS characterization of the particles in the ultraviolet spectral zone was recorded as an absorption spectrum, using which the properties of the NSTC particles can be easily calculated via the UV-VIS absorption wavelength. The instrument was operated in the wavelength range of 200 – 800 nm at a scanning speed of 600 nm/min using xenon flash lamp as the light source.

2.2.6 TG analysis

STA3700 (hHITACHI) thermogravimetric analyzer was employed to analyse the thermal stability of the NSTC particles by determining the weight loss with increasing temperature. The mass of the sample taken was 13.240 mg. The samples were heated between 40 ºC and 750 ºC at a ramp rate of 20º C/min under Nitrogen (N_2) atmosphere. The flow rate of N_2 gas was maintained at 100ml/min while the room temperature was maintained between 25º - 30º C throughout the experiment. To reduce errors in the measurement, the experiment was performed twice to confirm the repeatability of the test value. Moreover, DSC experiments were carried out to determine the phase change in the samples and the DTG technique was used to determine the maximum weight loss of the sample as a function of temperature, with respect to the thermo-gravimetric analysis.

2.2.7 FT-Raman spectroscopy

FT-RAMAN is a form of Raman Spectroscopy that adapts Fourier Transform techniques. The bands and bonds of carbonaceous NSTC particles were c*har*acterized by FT-RAMAN Spectrometer using a Bruker RFS 27 Multi RAM equipment by varying the wavenumber in the range of 4000-50 cm^{-1}. The Nd-YAG 1064 nm laser medium was used as a light source to focus the NSTC particles through the microscope via a 50X magnification objective lens. The intensities of the defect band (I_D) and graphitization band (I_G) peaks were identified and the ratio of I_D/I_G was determined to identify the structural defects in the NSTC particles at the atomic level. The results of the Raman spectra obtained in this study were averaged for 10 accumulations.

2.2.8 WCA measurements

The NSTC samples having a mean pore diameter of ~8 nm (mesoporous) was compressed into pellets by application of a pressure of 1.5 ton to prevail over a smooth surface. More than 4 pellets were prepared to repeat the test to eliminate inconsistent values and to measure the time dependent contact angle of water from 0 – 15 minutes with a 3-minute interval. WCA tests were performed by dropping liquid (distilled water) on the acquired pellet samples using Kyowa DMe-211 Plus Contact Angle Meter. The wettability of the NSTC particle was determined using sessile drop method by measuring the static contact angles. The contact angle (θ) of every single drop on the sample was examined and recorded by the FAMAS software. Two samples were tested for with five liquid droplets on each sample. Further, the surface energy (γ_S) of the NSTC particles was calculated using the Owens – Wendt – Rabel – Kaelble (OWRK) model.

3. Results and discussion

3.1 SEM and ball milling

Scanning Electron Microscope (SEM) measurements were carried out to evaluate the surface morphology and shape of the NSTC particles. The SEM images of the NSTC particles revealed a 2D structure with a well-defined interconnected network, as evidenced in Figs. 5(a)-(b). The particles not only exhibited uniform surface morphology and prominent agglomerates but also showed visuals of apparent spherical shape which is similar to that of carbon

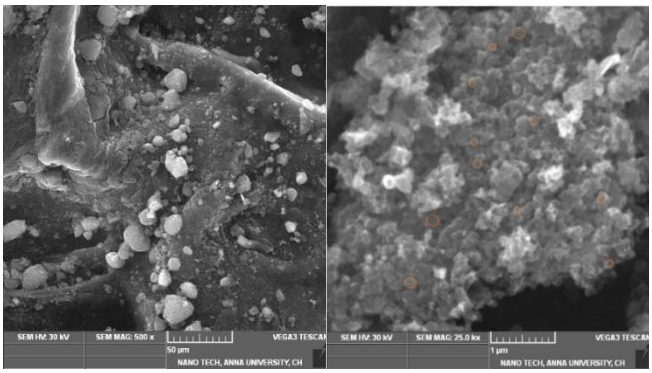

(a) Magnifications of 500X (b) Magnifications of 25kX

Fig. 5 SEM micrographs of the NSTC particles

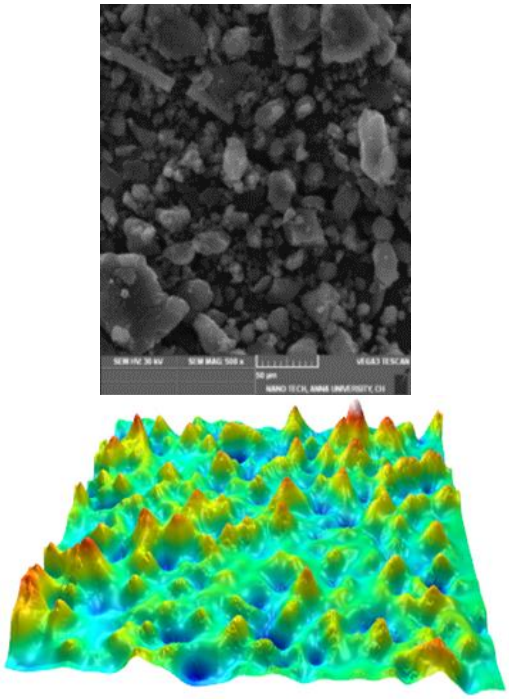

Fig. 6 SEM micrograph of the NSTC particles with the 3D-representation of their surface topography

black. Additionally, a stereoscopic reconstructed 3D surface topography of the NSTC particles depicted in Fig. 6 was used for effective qualitative visualization.

The NSTC particles collected directly from pyrolysis plant exhibited a heterogeneous size distribution with their sizes ranging from 82 nm to 173 nm, as evident in the SEM image in Fig. 7 a). Therefore, the planetary ball milling technique was employed to reduce the average size of the particles to less than 100 nm. The ball milling process was carried out in a trial basis by varying the speed and time. The desired outcome in terms of particle size was achieved at a rotation speed of 200 rpm and a milling time of 3 hours. The combined effects of acceleration and centrifugal forces in planetary ball milling led to intense grinding. As a result, the minimum, maximum and mean diameter of the NSTC particles decreased from 65 nm to 39.5 nm, from 178 nm to 77.5 nm, and from 112.8 nm to 55.6 nm, respectively. The ball milling technique also proved to be efficient in

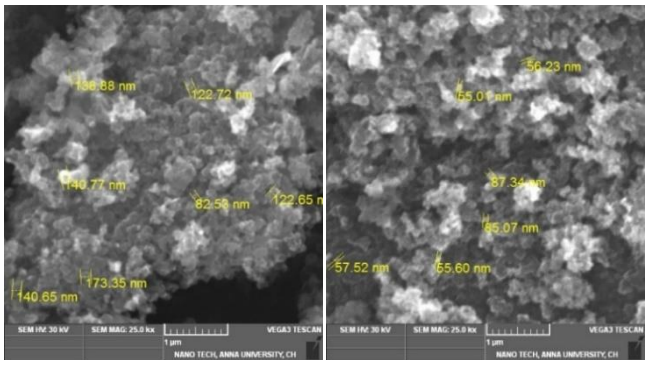

(a) Before ball milling (b) After ball milling

Fig. 7 Varying sizes of the NSTC particles

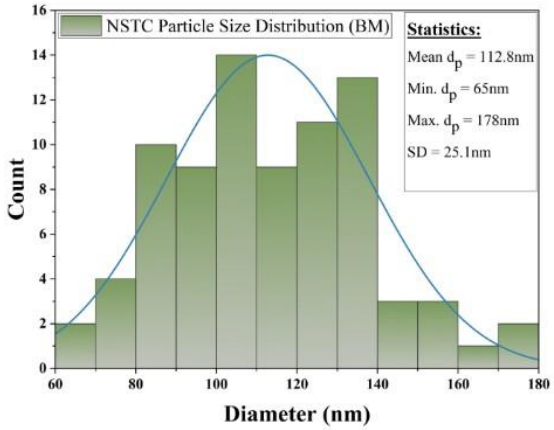

(a) Before ball milling

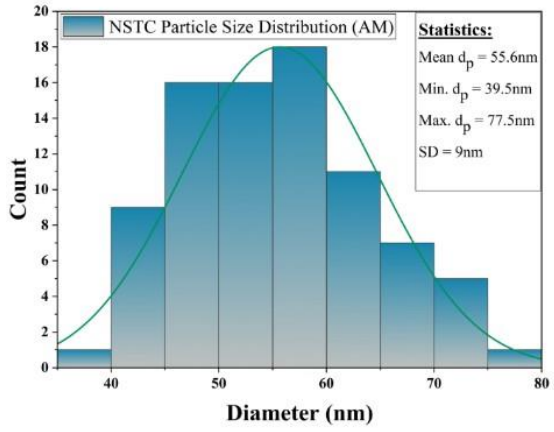

(b) After ball milling

Fig. 8 Size distribution and diameter statistics of the NSTC particles

reducing the standard deviation of the particle diameter from 25.1 nm to 9 nm. The outcome of the ball milling process resulted in a remarkable reduction in the size of the NSTC particles, as seen in Fig. 7 b) that represents the micrographs showing the size of the particle ranging between 55 nm and 87 nm (<100 nm) after the ball milling process. Corresponding to the micro-morphology and varying size of the NSTC particles, the histogram for the particle size distribution before and after ball milling as illustrated in the Figs. 8(a)-(b) was obtained through

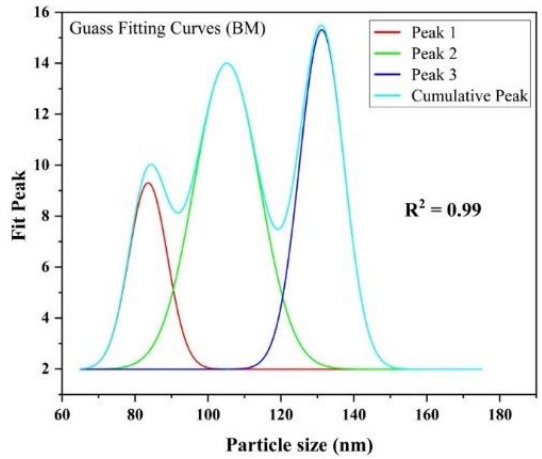

(a) Before ball milling

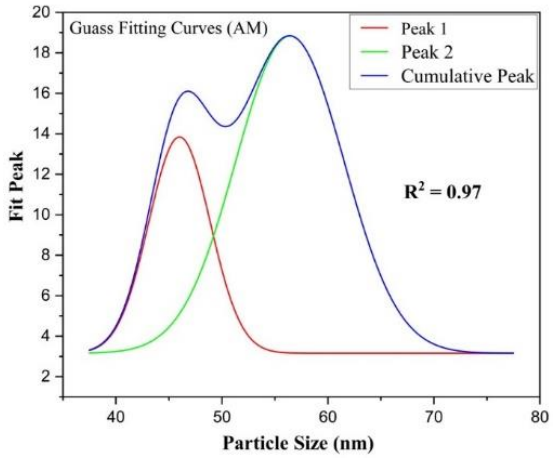

(b) After ball milling

Fig. 9 Non-linear curve fitting for the NSTC particle size using gauss model

statistical analysis. In addition, Gauss (non-linear) curves with 100% fitting accuracies as shown in Figs. 9(a)-(b) were obtained using the Levenberg Marquardt iteration algorithm, proving that the size of NSTC particles decreased when subjected to the planetary ball milling process. Comparison of the cumulative fit peaks of the NSTC particles (see Fig. 9) clearly indicates a significant reduction in the varying particle size after the ball milling process which will be an effective way compared to solvothermal process (Rosa *et al*. 2014).

Besides the successful reduction in the size of the NSTC particles, the ball milling process is also advantageous in reducing the agglomerates as evident from Figs. 10(a)-(b) that show the SEM images of the agglomerated particles present in abundance before ball milling and the reduction in the agglomerate size after ball milling, respectively. Eventually, this complete process of ball milling resulted in obtaining nano sized material from tyre char in the form of NSTC particles as validated through SEM analysis.

3.2 CHNSO elemental analysis

NSTC particles are carbonaceous materials having rich carbon content that gets deposits over the surface of the

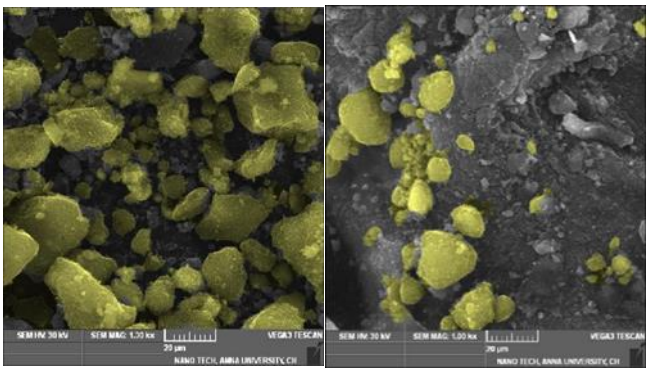

(a) Large agglomerated particle before ball milling

(b) Reduced agglomerated particles after ball milling

Fig. 10 Agglomerated state of NSTC particles

char during the pyrolysis process. Inherently, the presence of carbon content varies according to the type of tyre and the pyrolysis conditions (temperature, time, & pressure). Hence, CHNSO test was performed to determine the composition of Carbon (C), Hydrogen (H), Nitrogen (N), Sulphur (S), and Oxygen (O) present in the NSTC compound. Table 3 presents the CHNSO concentration of the NSTC particles determined by the elemental analyzer. It is evident that the NSTC material has a high carbon content and a significant amount of Sulphur (3.3 %) indicates the solid residual part. Nevertheless, the small portion of hydrogen in the solid shows that the NSTC particles are less reactive and form few C-H bonds. It is to be noted that the appearance of hydrogen will be greater in gases and liquids (Paul *et al*. 2023) that are obtained from the tyre pyrolysis process. Further, the molecular mass (180.64 g/mol) and the basic empirical formula ($C_{102}H_{21}NS_2O_{25}$) of the NSTC compound were determined using their respective atomic masses given in the periodic table. CHN test results revealed that the NSTC had high carbon content with less impurities. Therefore, NSTC particles could be directly utilized in cement composites to improve the conductivity inside the matrix.

3.3 XRD

XRD is a technique used to characterize nanomaterials for the purpose of phase identification of different minerals. It offers the advantage of probing the polymorph crystallinity and the crystallite size of the nanomaterials (Barhoum *et al*. 2018). The crystal structure of the NSTC particles was analysed by calculating the d-spacing (d) and crystallite size (D), using Bragg's Law and Debye-Scherrer equation, respectively, as given in Eqs. (1)-(2). Additionally, the crystallinity of the NSTC particles was determined using Eq. (3).

Bragg's Law λ

$$d = \frac{\lambda}{2 \sin \theta} \tag{1}$$

Debye-Scherrer Equation

$$D = \frac{K \lambda}{\beta \, Cos \, \theta} \tag{2}$$

Table 3 Comparison of the composition of NSTC particles acquired by CHNSO analysis

Sample	CHNSO Analysis							References
	C (%)	H (%)	N (%)	S (%)	O (%)*	C/N ratio	C/H ratio	
NSTC particle	71.28	1.250	0.82	3.3	23.35	86.89	57.04	Current work
CBp	52.25	2.177	0.20	1.839	43.534	-	-	(Paul *et al*. 2023)

* Oxygen (O) % was determined by subtraction of C %, H %, N %, & S % from total composition (100%)

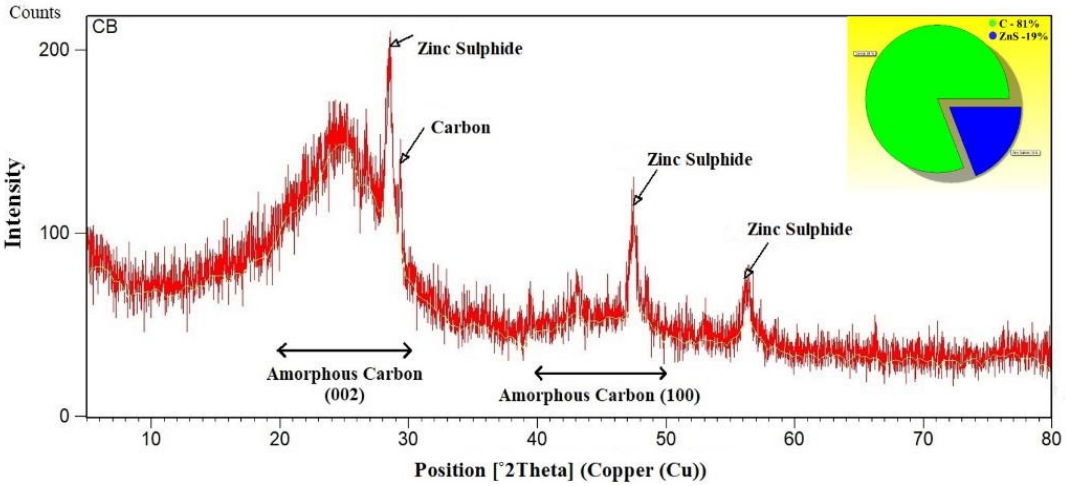

Fig. 11 XRD pattern for phase identification and quantification of NSTC particles

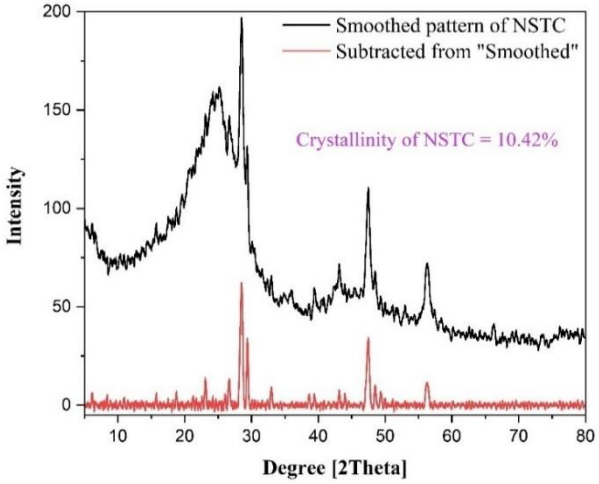

Fig. 12 XRD pattern of the NSTC particles to determine the crystallinity

where, K = Scherrer constant (0.94), λ = Wavelength of X-Ray beam used (1.54Å), β is the Full Width at Half Maximum (FWHM) of the peak, θ is the Bragg angle.

Crystallinity (%)

$$Crystallinity = \frac{Area\ of\ crystalline\ peaks}{Area\ of\ all\ peaks\ (amorphous\ and\ crystalline)}\ X\ 100 \quad (3)$$

The XRD pattern of the NSTC particles was analysed to identify the presence of major crystalline mineral phases. Further, the pattern also aided in assessing the crystallite size (Uvarov and Popov 2007, 2013) and purity of the material. Fig. 11 shows the phase identification of the NSTC particles along with its quantification chart that confirms the purity of carbon. The intense diffraction peaks (2θ) of the NSTC particles were observed and matched with the JCPDS cards (01-072-2091 & 01-077-2100) to identify the mineral compounds. It was found that preponderance of the peaks could be attributed to Zinc sulphide (ZnS), since Zinc Oxide (ZnO) was used as a catalyst in production of tyres and to ZnS that was formed during the pyrolysis treatment due to sulfidation (Shilpa *et al*. 2018, M. Wang *et al*. 2019). The 2θ values of 28.52º, 47.49º, and 56.12º correspond to the reflections from (111), (220), and (311) planes, respectively, of the ZnS phase orchestrated from ZnO which is a semi-conducting material Rai and Bajpai (2023). On the other hand, the functional group of pure carbon present at 29.37º corresponds to the diffraction from the (110) plane. Furthermore, the diffractogram showed two broader diffraction peaks between 20º - 30º and 40º - 50º. The first and second broader peaks are attributed to the Miller planes (002) and (100), respectively, which represents the existence of amorphous carbon structure with arbitrarily arranged microcrystalline graphitic carbon (Singh *et al*. 2016, Nogueira *et al*. 2019). The particles possess graphite as evident from the quite intense peak at 2θ value of 26º (Papanikolaou *et al*. 2021). Graphite exhibits good electrical conductivity. Besides, the crystallite size of the NSTC particles calculated using the Debye-Scherrer equation was less than 100 nm at all space groups. In this case, the average crystallite size (nm) of the NSTC particles was found to be ~35 nm. The parameters of NSTC particle structure derived from the XRD pattern after ball milling is summarized in Table 4. In addition, the percentage of polymorph crystallinity (10.42%) of the NSTC particle was

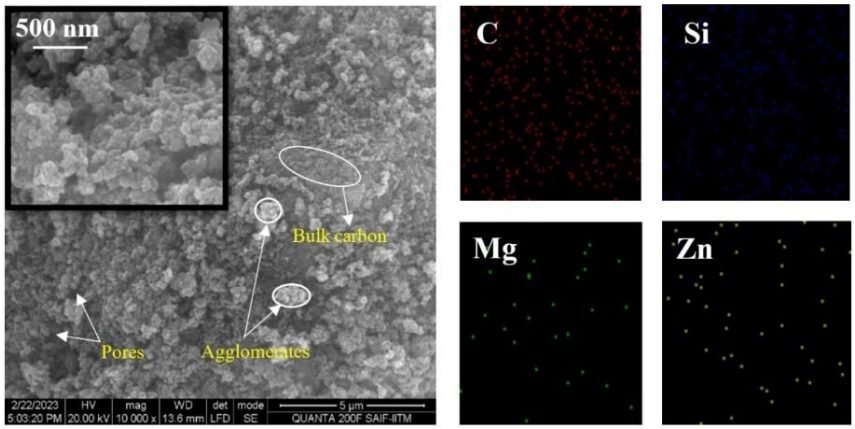

Fig. 13 HR-SEM images of the NSTC particles along with maps of C, Si, Mg, Zn

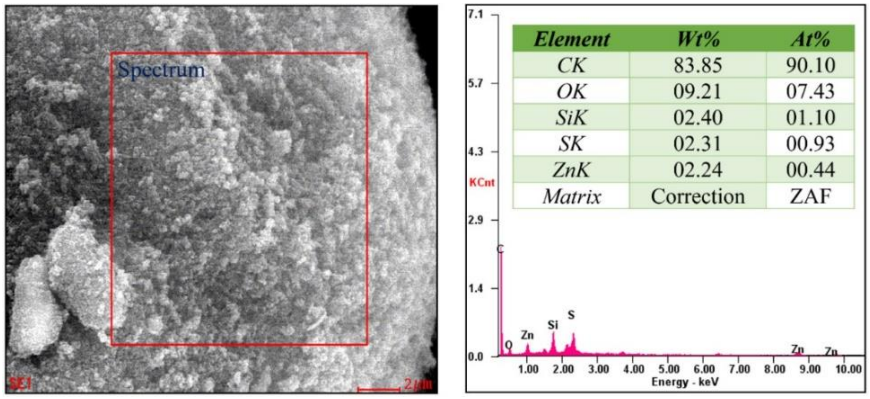

Fig. 14 HR-SEM image of NSTC particle with EDAX data

Table 4 XRD parameters of NSTC particles obtained from pyrolysis treatment

Plane	Position [°2θ]	Height [cts]	FWHM [°2θ]	d-spacing [Å]	Relative Intensity [%]	Crystallite size [nm]
002	24.94330	39.07542	0.13420	3.56981	42.30	60.62803
111	28.52762	92.37977	0.39360	3.12897	100.00	20.82569
110	29.37534	47.85228	0.23616	3.04057	51.80	34.77583
100	43.67623	66.56900	0.13520	3.55627	72.06	63.30219
220	47.49071	56.73391	0.47232	1.91455	61.41	18.37529
311	56.128160	25.89901	0.55104	1.63869	28.04	16.33788

determined from the XRD pattern, as shown in Fig. 12. Finally, the presence of high carbon content was validated by the peaks ascribed to (110), (002), and (100). Therefore, incorporating NSTC particles with amorphous carbon in cement composites will enhance the strength, durability, and electrical conductivity of these composites. Nevertheless, the presence of ZnS in NSTC particles may lead to the degradation of the cement over time and hence, care must be taken to remove ZnS by adopting suitable chemical treatments.

3.4 HR-SEM / EDX / Mapping

The physical structure, morphology, and miscellaneous elemental composition of the NSTC particles are the potential factors that are determined from the HR-SEM/ EDX measurements. Figures 13 and 14 show the HR-SEM images of NSTC particles along with the elemental mapping and the EDX, respectively. Fig. 13 reveals the dense and homogeneous features of the NSTC particles containing less bulk carbon. However, aggregated particles formed by sulfidation treatment during tyre pyrolysis were visible as agglomerates (Dwivedi *et al*. 2020). The picture-in-picture shown in Fig. 13 also represents the HR-SEM image at a scale of 500 nm showing the nano spherical shaped morphology of the particles connected with each other and having an approximate particle size of 50 nm. On the other hand, the surface of the NSTC particles was found to be rough which justifies the existence of inorganic substances mixed during the tyre compounding process. Furthermore, the distribution of various elements such as Carbon (C), Magnesium (Mg), Silica (Si), and Zinc (Zn)

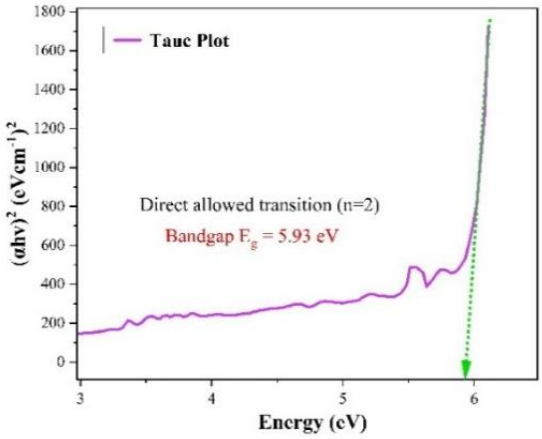

(a) Direct allowed transition

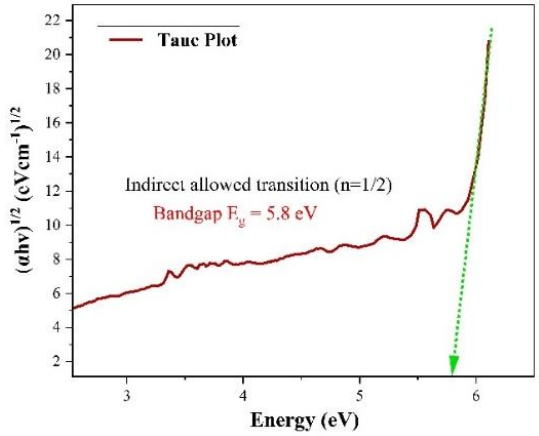

(b) Indirect allowed transition

Fig. 15 Determination of bandgap using Tauc method

present in NSTC particles are represented by mapping images (Fig. 13). From EDX analysis and the corresponding mapping, the presence of Oxygen (O) content and Si may result in the formation SiO_2 substance (Jiang *et al*. 2022), while the very least distribution of Mg indicates the less impurities contained in sample.

The EDX analysis of the NSTC particles was carried out using X-Ray series with 'K' characteristics (Feng *et al*. 2021). The five prominent intense peaks in the EDX spectrum represent the K-series of the Carbon component (CK), the K-series of the Oxygen component (OK), the K-series of the Silica component (SiK), the K-series of the Sulphur component (SK), and the K-series of the Zinc component (ZnK), wherein the carbon element was identified to be the major component of the NSTC particles. The quantitative elemental analysis performed using EDX on Fig. 14 estimated the relative quantities of C, O, Si, S, and Zn in both weight and atomic percentage. The EDX elemental spectrum provides the necessary evidence to substantiate the claim that NSTC particles are carbon governed materials that possess high content of carbon atoms (~ 90 %), which is higher than that found in commercial graphene oxide (Huang *et al*. 2012). The results also indicate the presence of significant Si content in the NSTC particles which was appropriate for the dense polymerization formation (Long *et al*. 2018), while the other trace elements, namely S and Zn account for a very small portion of about 2.31 wt.% and 2.24 wt.%, respectively. The presence of the inorganic substances namely, Zn and S also explains the presence of ZnS as agglomerated clusters (Nogueira *et al*. 2019), which has been previously confirmed by XRD analysis. The EDX analysis also provided the ratio of carbon to oxygen (Hu *et al*. 2017). The elemental mapping and EDX spectrum together provided evidence for the presence of high carbon content in the NSTC particles. HR-SEM micrographs of the NSTC particles revealed the spherical or ellipsoidal structure and the presence of agglomerates in the form of spheres that imitates the structure of commercial carbon black. Despite certain obvious differences between NSTC particles and carbon black for instance, in the uneven particle size and shape, eventually, NSTC particles, with their nano-size and dominant carbon content, have the potential to revolutionize the construction industry by functioning as a sustainable nanomaterial.

3.5 UV-VIS Spectroscopy

The band structure and its corresponding energy gap are important parameters of a semiconductor material that demonstrate their electrical conductivity (flow of electrons). In general, the band gap/energy gap [E_{gap} (eV)], which is the distance between the valence and the conduction bands, is determined from the UV-VIS absorption spectrum. Consequently, the band gap (E_g) of the NSTC particles was determined from the absorption spectrum by the Tauc's method using Eqs. (4)-(6) (Tauc *et al*. 1966, Tauc and Scott 1967, Dahrul *et al*. 2016, De Falco *et al*. 2021, Al-Fa'ouri *et al*. 2023).

$$(\alpha hv) = \beta(hv - E_g)^n \tag{4}$$

$$(\alpha hv)^{1/n} = \beta(hv - E_g) \tag{5}$$

$$\alpha = \frac{2.303 \times A}{l} \tag{6}$$

where, E_g is the energy gap, α is the molar absorptivity, h is the Planck's constant, v is the frequency of light, and n depends upon the type of transition and electron density. In equation (5), n = 2 for direct allowed transition, n = 1/2 for indirect allowed transition, n = 2/3 for forbidden direct transition, and n = 1/3 for forbidden indirect transition. Since NSTC particles possess high carbon content, the nature of transition such as direct and indirect allowed transition is solely determined by relating $(\alpha hv)^2$ and $(\alpha hv)^{1/2}$, respectively to hv. Therefore, the direct and indirect allowed bandgap energies were determined by extrapolating the linear part of the Tauc plot to intersect the point along the y-axis at which $(\alpha hv)^2$ and $(\alpha hv)^{1/2}$ is equal to zero (Dahrul *et al*. 2016, Al-Fa'ouri *et al*. 2023). Figs. 15(a)-(b) represent the bandgap energies of the NSTC particles from the intersection point as E_g = 5.93 eV (direct bandgap) and E_g = 5.8 eV (indirect bandgap). The nearer bandgap values of both the allowed transition (direct and indirect) indicates the certainty of NSTC particle. In

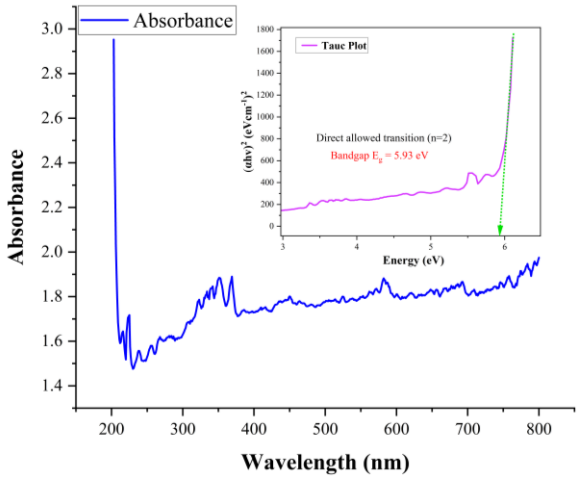

Fig. 16 UV-VIS absorption of NSTC particles with Tauc's plot (direct bandgap) in the inset

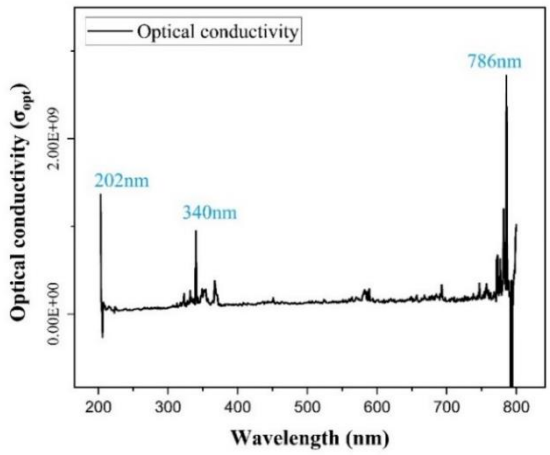

Fig. 17 Optical conductivity variation of the NSTC particle with UV-VIS absorption wavelength

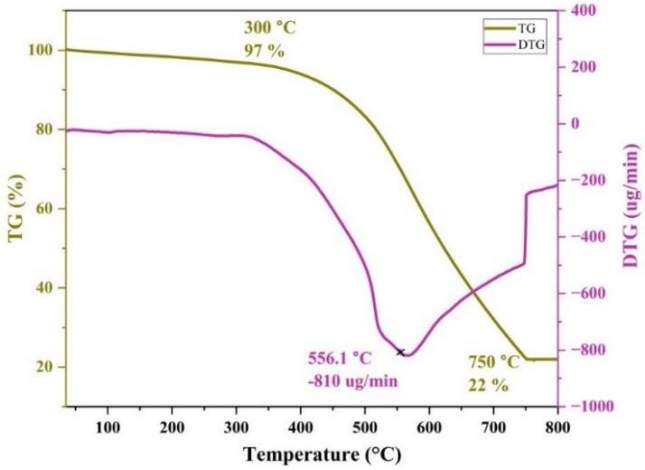

Fig. 18 TG and DTG plots for the NSTC particles

this study, the direct bandgap energy (E_g = 5.93 eV) was used with the results of the absorption spectrum, as represented in Fig. 16. Due to the wide nature of the bandgap (>2 eV), larger external energy is required for the electrons to enter the conduction band. The wide energy gap is mainly due to the presence of amorphous phases in the material (as confirmed from XRD analysis) and the quantum size effect, which leads to minimum heat accumulation. Nevertheless, the nature of NSTC particles articulates their lower electrical resistance and superior conductivity. Furthermore, the UV-VIS absorption spectrum of NSTC particles in Fig. 16 reveals the pure carbon characteristics of these particles as evident from the display of good absorbance throughout the wavelength range of 200 nm to 800 nm. The absorption coefficient or molar absorptivity (α) of the material was determined from Eq. (6). Therefore, incorporating wide bandgap NSTC particles as nano materials into cementitious composites is expected to improve the electrical conductivity and opens up the possibility for the development of self-sensing structures.

The optical conductivity is a crucial parameter to determine the electronic state of a material. It is quite closely related with the dielectric function and depends upon the optical bandgap, refractive index, absorption coefficient, incident photon frequency, and extinction coefficient. The optical conductivity is obtained from the Beer-Lambert law by analysing the UV-Vis absorption spectrum. Therefore, the optical conductivity of the NSTC particles is calculated using the Eqs. (7)-(10).

$$\sigma_{opt} = \frac{\alpha\, n\, c}{4\,\pi} \tag{7}$$

$$\text{Where, } \alpha = \frac{2.303 \times A}{l} \tag{8}$$

$$n = \frac{1}{T_s} + \sqrt{\frac{1}{T_s - 1}} \tag{9}$$

$$T_s = 10^{(-A)} \times 100 \tag{10}$$

where, σ_{opt} is the optical conductivity, α is the absorption coefficient, n is the refractive index, c is the speed of light in vacuum, A is the absorbance, and T_s is the transmitted intensity.

The UV-Vis absorption plot as depicted in Fig. 17 portrays the variation of the optical conductivity of the material as a function of the absorption wavelength. The optical conductivity initially increased at 202 nm as the wavelength increased. When the wavelength of light approached, an insignificant decrease in optical conductivity at 250 nm was observed that can be neglected. Meanwhile, the optical conductivity started to increase when the light wavelength further approached 340 nm and stayed positively stable through 750 nm. The maximum optical conductivity was noticed at 786 nm. Subsequently, the conductivity suddenly decreased and then rose to a stable value between 790 nm and 800 nm. The observed results from the absorption spectrum describes the occupied electronic state of the NSTC particles which is confirmed from the optical conductivity values.

3.6 TG analysis

Nanoscale materials are critical at elevated temperature as it can affect the mechanical properties of cement matrix

Table 5 Thermal parameters calculated from DSC data for phase change of the NSTC particle

First Phase transformation			Second Phase transformation		
Crystallization range		Enthalpy of crystallization	Crystallization range		Enthalpy of crystallization
T_i ºC	T_f ºC	ΔH_{crys} (mJ/mg)	T_i ºC	T_f ºC	ΔH_{crys} (mJ/mg)
300	411	146	412	300	411

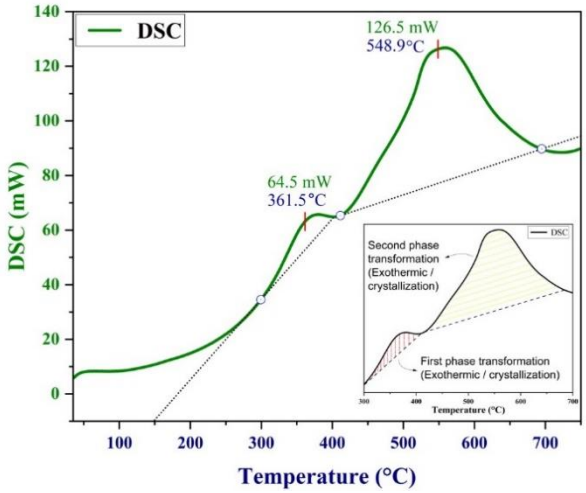

Fig. 19 Thermal analysis (DSC) of the NSTC particles

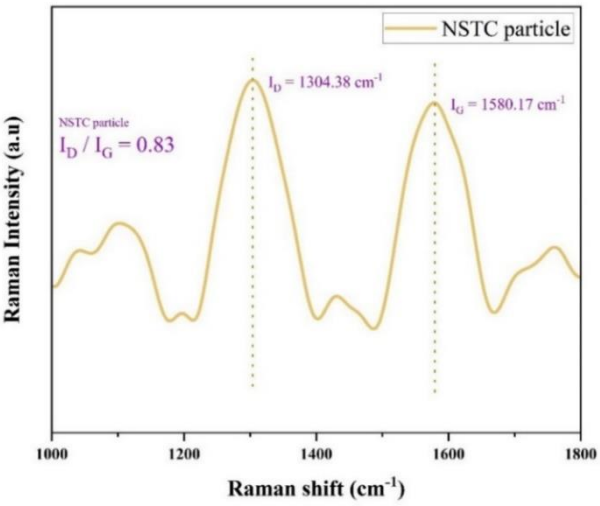

Fig. 20 FT Raman spectrum of the NSTC particles indicating the I_D/I_G ratio

due to degradation of hydration products Lim and Mondal (2014). Therefore, the TGA and DTG measurements were performed at a heating rate of 20 ºC/min to determine the mass loss and thermal degradation, respectively of the NSTC particles. Fig. 18 shows the TG and DTG plots of the NSTC particles. The TGA curve recorded three different intervals of mass loss regions. In the initial region, a preliminary weight loss of 3% was observed for temperatures between 35 ºC and 300 ºC, which can be ascribed to the removal/evaporation of adsorbed water and moisture content in the pores of NSTC particles. The increased weight loss rate was observed in the second region ranging for temperatures ranging from 300 ºC to 750 ºC, indicating the devolatilization process (removal of O, N, & H) as justified by CHNS analysis (low content of O, N, & H) followed by the combustion of fixed carbon and volatile components Kok and Özgür (2013) in the NSTC particles. In the last interval (750 ºC to 800 ºC), the TGA curve showed no further noticeable breakdown as the material became thermally stable due to slow combustion. Certainly, the high combustion temperature of 750 ºC of the NSTC particles indicate their high thermal stability (Khalid *et al.* 2022). In addition, the unreacted particles account for the presence of silica content in the ash residue after the combustion process Demirbas (2004), as indicated in the HR-SEM mapping (Fig. 13). DTG recorded the highest weight loss in the TG curve. The maximum weight loss rate for the NSTC particles at 556.1 ºC determined from the inflection point in the DTG plot of Fig. 18 was found to be -810 µ/min. Moreover, it was observed that the rate of thermal degradation increased gradually after 600 ºC. The DSC curve plotted in Fig. 19 represents the phase transformation of the material. The two peaks in the DSC curve at 361.5 ºC and 548.9 ºC indicate the two different stages of exothermic phase transformation that took place in the material which resists corrosion rate of the material (Torres *et al.* 2021). Further, DSC plots were analysed to calculate the thermodynamic parameters such as enthalpy and temperature range of crystallization for both the phase transformations. The values are given in Table 5. Eventually, the interpretation of the results of the TG, DTG, and DSC measurements indicated the presence of a substantial amount of carbon in the NSTC particles with less ash residue due to dominant combustion process.

3.7 FT – Raman

The FT-Raman spectroscopy, a powerful technique for the characterization of nanostructured materials, demonstrates the explicit relation between bands and bonds. This technique was used to determine the structural defects (I_D/I_G ratio) and the type of bonds present in the NSTC particles. The Raman spectrum shown in Fig. 20 revealed the presence of two standard peaks referred to as the Defect band (I_D = 1304 cm^{-1}) and the Graphitization band (I_G = 1580 cm^{-1}) and are identical with that found in other reports (Maroufi *et al.* 2017, Wang *et al.* 2019, Adar 2022). The presence of I_D indicates the existence of a defected crystal structure in the material owing to breathing vibration mode or in-plane termination of the disordered carbon ring, while I_G indicates the presence of graphite in a 2D hexagonal lattice that corresponds to the carbon system of regular C=C bonds and sp^2 vibration. It is also used to evaluate the material quality (Wang *et al.* 2019, Khalid *et al.* 2022).

Accordingly, the FT-Raman spectrum of the NSTC particles (Fig. 20) revealed a clear I_D around 1304 cm^{-1} and

Table 6 Time dependent contact angle of NSTC particles for water and Di-iodomethane

Time (ms)	V_o (µl)	Water		Di-iodomethane	
		Average C.A. Left (Degree)	Average C.A. Right (Degree)	Average C.A (Degree)	Average C.A (Degree)
1000	5	145.3	143.1	144.2	105.3
61000	5	143.1	142.8	142.9	103.6
121000	5	141.8	141.7	141.7	102.2
181000	5	140.8	140.8	140.8	100.8
241000	5	140	140.7	140.4	98.1
301000	5	138.8	139.9	139.4	97.6

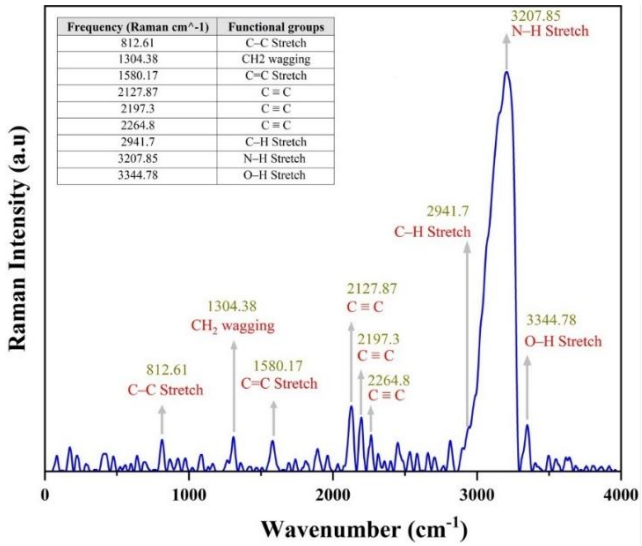

Fig. 21 FT Raman spectra showing the assigned functional groups in the NSTC particles

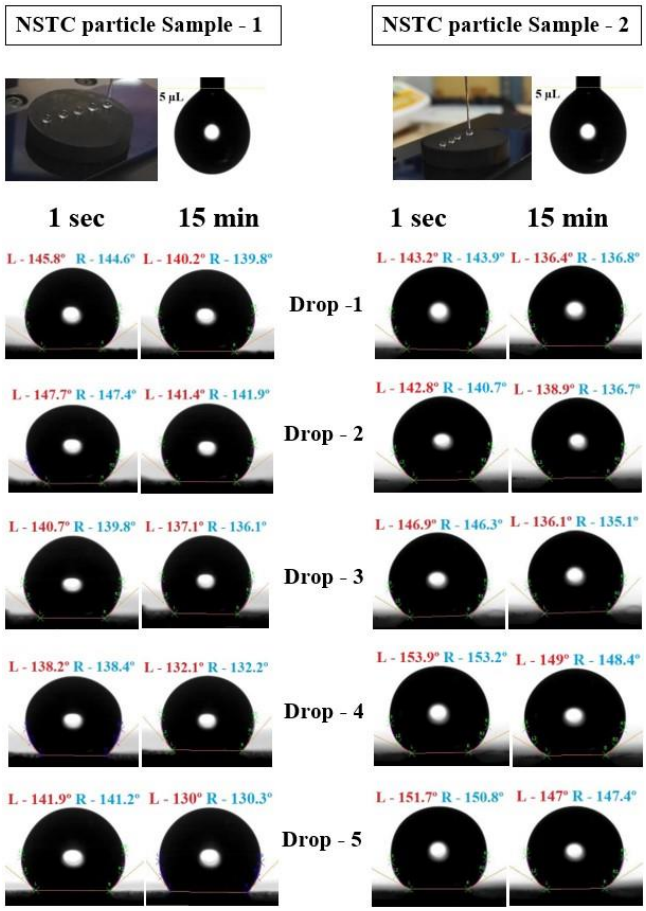

Fig. 22 Time dependent water contact angles of the NSTC particles using sessile drop method

I_G around 1580cm^{-1} indicating the presence of disordered carbon content and 2D graphene lattices, respectively. In addition, residence of both the bands shows that the carbon content is turbostratically disordered (M. Wang *et al*. 2019). It was observed that the intensity of the defect band was slightly higher than that of the graphitization band indicating NSTC to be a qualified carbon material Adar (2022) with small defects in the graphitic structure (Maroufi *et al*. 2017). Furthermore, the estimated I_D/I_G ratio for the NSTC particles was estimated to be 0.83, further establishing the presence of obvious structural defects at the atomic level. The ratio was found to be comparable to the values obtained from similar studies reported on pyrolytic waste tyres (Mahmood *et al*. 2020, Khalid *et al*. 2022). Therefore, the NSTC particles with I_D/I_G ratio of 0.83 can function as an effective nano reinforcing filler by establishing a strong interfacial bond with the cementitious matrix. Such a higher ratio of I_D/I_G confirms the sustainable nature of nano carbon filler that proves to be a promising alternative to commercial nanomaterials.

The FT-Raman spectrum plotted in Fig. 21 depicts the discrete functional groups on the surface of the NSTC particles pyrolyzed from tyre waste. The Raman shift (in cm^{-1}) characterizes the bonding efficiency and provides information about the vibrational frequency modes that help to identify and detect the type of bonds present in the material Adar (2016). The peak at a wavenumber of 3344.78 cm^{-1} indicates the presence of O – H bond stretch (hydroxyl groups) attributed to the existence of alcohol functional group (Figueredo *et al*. 2017). The wavenumber 3207.85 cm^{-1} having an intense peak characterizes the N – H stretch which is broadened and shifted by the H-bonding. The peak observed at 2941.7 cm^{-1} is attributed to the C – H stretch (methylene group), confirming the incomplete carbonization of cellulose during pyrolysis (Chia *et al*. 2012). In the region between 2300 – 2100 cm^{-1}, the peaks at 2264.8 cm^{-1}, 2197.3 cm^{-1}, and 2127.87 cm^{-1} are attributed to C ≡ C bond. The low intensity peaks at wavenumbers of

Table 7 Surface energy and their components of model liquids

Model liquid	γ_L (mJ/m^2)	γ_L^d (mJ/m^2)	γ_L^p (mJ/m^2)	References
Water	72.8	21.8	51	Fowkes (1964)
Di-iodomethane	50.8	50.8	0.0	(Gindl *et al*. 2001)

Table 8 Surface energy of NSTC particle and the values of their components

Sample	Time (ms)	γ_S (mJ/m^2)	γ_S^d (mJ/m^2)	γ_S^p (mJ/m^2)
NSTC particle	1000	7.58	6.98	0.600
	61000	8.01	7.43	0.578
	121000	8.47	7.90	0.565
	181000	8.97	8.39	0.575
	241000	10.08	9.37	0.706
	301000	10.60	9.89	0.710
Average Surface energy		8.95	8.33	0.622

1580.17 cm^{-1}, 1304.38 cm^{-1}, and 812.62 cm^{-1} indicate the C = C bond stretch arising due to the presence of carbonized material (Chia *et al*. 2012), CH_2 wagging, and C – C bond stretch with complex molecules, respectively. These functional group, especially the carboxyl groups in the NSTC particles, are expected to establish strong interactions with the cement matrix.

3.8 WCA measurement

The variations in the contact angle of the NSTC pellets over time were measured using water and Di-iodomethane at room temperature using the sessile drop technique and the tangent method with automatic detection of drop transition. The water contact angle (θ) was measured for a time period of 15 min at 3 min interval for a total of 2 pellets with five water droplets on each sample. A water droplet of volume 5 µl was placed on the test samples and the static contact angle was measured. Fig. 22 shows the time dependent contact angle (θ) values of the NSTC pellets revealing the changes over time (1 sec and 15th min). Table 6 summarizes the values of the contact angle for water and Di-iodomethane at different times. A reduction in water contact angle from 144.2º to 139.4º was observed as time progressed from 1sec to 15min. This is an indication of the hierarchical structure possessing nano patterns. Therefore, NSTC particles were found to be nano structured materials with highly hydrophobic surfaces, similar to carbon nanotube (Goh *et al*. 2014). This in turn indicates a lower interaction between water and NSTC particles which requisites the use of chemical admixtures (polycarboxylate) to disperse the NSTC material in the cement matrix.

Surface energy or surface tension of the material was determined pertaining to the contact angles (with time variation) by employing the Owens -Wendt – Rabel – Kaelble (OWRK) D.K. Owens (1969) theoretical model. The OWRK model is an extended Fowkes model (Fowkes, 1962) that was proposed based on the Young-Dupree equation (Rbihi *et al*. 2020, Çıtak and Yarbaş 2022). By employing the values of contact angle, the surface tension (γ_S) of the NSTC particles was predicted with their respective dispersive γ_s^d and polar γ_s^p components using Eqs. (11)-(12).

Young-Dupree equation, OWRK model based on Eq. (11),

$$\gamma_L \, Cos\, \theta = \gamma_S - \gamma_{SL} \tag{11}$$

$$\gamma_L \, (1 + \cos\theta) = 2 \times \left(\sqrt{\gamma_S^d \gamma_L^d} + \sqrt{\gamma_S^p \gamma_L^p} \right) \tag{12}$$

where, γ_L is the surface free energy of the liquid (mJ/m^2), γ_S is the surface free energy of the solid (mJ/m^2), γ_{SL} is the surface free energy of the solid-liquid interface (mJ/m^2), θ is the angle of contact between the liquid and the solid surfaces (º), γ_S^d and γ_L^d are the dispersive surface free energies of the solid and liquid (mJ/m^2), respectively, γ_S^p and γ_L^p are the polar surface free energies of the solid and liquid (mJ/m^2), respectively.

Additionally, the contact angle of a model liquid, Di-iodomethane (non-polar solvent), with known dispersive and polar components was measured to support the determination of the surface energies of the NSTC particles. Tables 7 and 8 show the surface energies of the liquid as reported in literature and the NSTC particles, respectively. According to Table 8, the average surface energy of the NSTC particles is 8.95 mJ/m^2. To the best of the authors knowledge, there are no studies that report the determination of surface energy of NSTC particles using the contact angle method. This approach of calculating the total surface free energy with dispersive and polar components gives clear results compared to other theoretical approaches. In the context of nanosized construction materials, the low surface energy of the NSTC particles may affect their interaction with cementitious materials. However, a suitable surface treatment can enhance the surface energy of the NSTC particles and help in improving their performance such as bonding, capillary action, and interaction properties with other construction materials.

4. Conclusions

This experimental study lays the foundation for utilizing tire char as carbon nanomaterial to aid in the development of smart cement sensor composite. The various characterization results highlight the potential of NSTC particle having high amorphous carbon with multifunctional properties. The characterization results revealed that the wide bandgap energy (5.93 eV) due to quantum size effect has the ability to improve electrical conductivity. Furthermore, the intensity ratio of defect band to graphitization band (I_D/I_G = 0.83) of the NSTC particle indicates better bonding structure and presence of self-sensing property. Therefore, NSTC particle with such properties have the ability to improve the sensing property in the cement matrix to develop smart cement-based sensor composites for structural health monitoring and will be an alternate to commercial nanomaterials.

Acknowledgment

The authors would like to thank the Dean-School of Civil Engineering, Vellore Institute of Technology, Chennai, India, for providing support and lab facilities to carry out this research. We thank the "DST and SAIF/IIT/M", "Centre for Nanoscience and Technology, Anna University", "STIC CUSAT", "National Centre for Earth Science Studies – Thiruvananthapuram", "School of Advanced Sciences, VIT-Chennai", for providing the analytical services. We would like to acknowledge "Dr. Shanmuga Sundaram, VIT-Chennai", for providing valuable ideas during the research phase.

References

Abbas-Abadi, M.S., Kusenberg, M., Shirazi, H.M., Goshayeshi, B. and Van Geem, K.M. (2022), "Towards full recyclability of end-of-life tires: Challenges and opportunities", *J. Clean. Prod.*, **374**, 134036. https://doi.org/10.1016/j.jclepro.2022.134036.

Adar, F. (2016), "Introduction to interpretation of raman spectra using database searching and functional group detection and identification", *Spectroscopy*, **31**(7), 16-23.

Adar, F. (2022), "Use of raman spectroscopy to qualify carbon materials", *Spectroscopy*, **37**(6), 11-15, 50. https://doi.org/10.56530/spectroscopy.wx3481u2.

Al-Fa'ouri, A.M., Lafi, O.A., Abu-Safe, H.H. and Abu-Kharma, M. (2023), "Investigation of optical and electrical properties of copper oxide - polyvinyl alcohol nanocomposites for solar cell applications", *Arab. J. Chem.*, **16**(4), 104535. https://doi.org/10.1016/j.arabjc.2022.104535.

Banasiak, L., Chiaro, G., Palermo, A. and Granello, G. (2019), "Recycling of end-of-life tyres in civil engineering application: Environmental implications", *Nucl. Phys.*, **13**(1), 104-116.

Barhoum, A., García-Betancourt, M.L., Rahier, H. and Van Assche, G. (2018), *"Physicochemical characterization of nanomaterials: Polymorph, composition, wettability, and thermal stability"*, Emerging Applications of Nanoparticles and Architectural Nanostructures, Elsevier, Netherlands.

Chaala, A., Roy, C. and Ait-Kadi, A. (1996), "Rheological properties of bitumen modified with pyrolytic carbon black", *Fuel*, **75**(13), 1575-1583. https://doi.org/10.1016/0016-2361(96)00143-3.

Chia, C.H., Gong, B., Joseph, S.D., Marjo, C.E., Munroe, P. and Rich, A.M. (2012), "Imaging of mineral- enriched biochar by FTIR, Raman and SEM - EDX", *Vib. Spectrosc.*, **62**, 248-257. https://doi.org/10.1016/j.vibspec.2012.06.006

Chen, C.C., Huang, Y. H. and Chien, H.J. (2021), "Waste tire-derived porous nitrogen-doped carbon black as an electrode material for supercapacitors", *Sustain. Chem. Pharm.*, **24**, 100535. https://doi.org/10.1016/j.scp.2021.100535

Çıtak, A. and Yarbaş, T. (2022), "Using contact angle measurement technique for determination of the surface free energy of B-SBA-15-x materials", *Int. J. Adhes. Adhes.*, **112**, 103024. https://doi.org/10.1016/j.ijadhadh.2021.103024.

Dahrul, M., Alatas, H. and Irzaman (2016), "Preparation and optical properties study of CuO thin film as applied solar cell on LAPAN-IPB satellite", *Procedia Environ. Sci.*, **33**, 661-667. https://doi.org/10.1016/j.proenv.2016.03.121.

Demirbas, A. (2004), "Combustion characteristics of different biomass fuels", *Prog. Energy Combust. Sci.*, **30**(2), 219-230. https://doi.org/10.1016/j.pecs.2003.10.004.

Dwivedi, C., Manjare, S. and Rajan K Sushil (2020), "Recycling of waste tire by pyrolysis to recover carbon black: an alternative reinforcing filler", *Compos. Part B*, **200**, 108346. https://doi.org/10.1007/s10163-023-01635-6.

De Falco, G., Mattiello, G., Commodo, M., Minutolo, P., Shi, X., D'Anna, A. and Wang, H., (2021), "Electronic band gap of flame-formed carbon nanoparticles by scanning tunneling spectroscopy", *Proc. Combust. Inst.*, **38**(1), 1805-1812. https://doi.org/10.1016/j.proci.2020.07.109.

Feng, Z., Zhao, P., Li, X. and Zhu, L. (2021), "Preparation and properties of bitumen modified with waste rubber pyrolytic carbon black", *Constr. Build. Mater.*, **282**, 122697. https://doi.org/10.1016/j.conbuildmat.2021.122697.

Feng, Z.G., Rao, W.Y., Chen, C., Tian, B., Li, X.J., Li, P.L. and Guo, Q.L. (2016), "Performance evaluation of bitumen modified with pyrolysis carbon black made from waste tyres", *Constr. Build. Mater.*, **111**, 495-501. https://doi.org/10.1016/j.conbuildmat.2016.02.143.

Figueredo, N.A. de, Consta, L.M. da, Melo, L.C.A., Siebeneichlerd, E. and Antônio, Tronto, J. (2017), "Characterization of biochars from different sources and evaluation", *Rev. Ciência Agronômica*, **48**, 395-403. https://doi.org/10.5935/1806-6690.20170046.

Fowkes, F.M. (1962), "Determination of interfacial tensions, contact angles, and dispersion forces in surfaces by assuming additivity of intermolecular interactions in surfaces", *J. Phys. Chem.*, **66**(2), 382. https://doi.org/https://doi.org/10.1021/j100808a524.

Fowkes, F.M. (1964), "Attractive forces at interfaces', *Ind. Eng. Chem.*, **56**, 40-52. https://doi.org/10.1021/ie50660a008.

Gao, N., Wang, F., Quan, C., Santamaria, L., Lopez, G. and Williams, P.T. (2022), "Tire pyrolysis char: Processes, properties, upgrading and applications", *Prog. Energy Combust. Sci.*, **93**, 101022. https://doi.org/10.1016/j.pecs.2022.101022.

Gindl, M., Sinn, G., Gindl, W., Reiterer, A. and Tschegg, S. (2001), "A comparison of different methods to calculate the surface free energy of wood using contact angle measurements", *Colloids Surf. A*, **181**, 279-287. https://doi.org/10.1016/S0927-7757(00)00795-0.

Goh, Y.M., Han, K.D., Tan, L.L. and Chai, S.P. (2014), "Facile preparation of superhydrophobic thin films using non-aligned carbon nanotubes", *Adv. nano Res.*, **2**(4), 219-225. https://doi.org/10.12989/anr.2014.2.4.219

Goksal, F.P. (2022), "An economic analysis of scrap tire pyrolysis, potential and new opportunities", *Heliyon*, **8**(11), e11669. https://doi.org/10.1016/j.heliyon 2022.e11669.

Hu, M., Yao, Z. and Wang, X. (2017), "Characterization techniques for graphene-based materials in catalysis", *AIMS Mater. Sci.*, **4**(3), 755-788. https://doi.org/10.3934/matersci.2017.3.755.

Huang, Z.D., Zhang, B., Liang, R., Zheng, Q. Bin, Oh, S.W., Lin, X.Y., Yousefi, N. and Kim, J.K., (2012), "Effects of reduction process and carbon nanotube content on the supercapacitive performance of flexible graphene oxide papers", *Carbon*, **50**(11), 4239-4251. https://doi.org/10.1016/j.carbon.2012.05.006.

IMARC (2022), *India Tyre market: Industry trends, share, size, Growth, Opportunity and Forecast 2023- 2028*, International Market Analysis Research and Consulting, Uttar Pradesh, India.

Jiang, G., Pan, J., Deng, W., Sun, Yanzhi, Guo, J., Che, K., Yang, Y., Lin, Z., Sun, Yancai, Huang, C. and Zhang, T. (2022), "Recovery of high pure pyrolytic carbon black from waste tires by dual acid treatment", *J. Clean. Prod.*, **374**, 133893. https://doi.org/10.1016/j.jclepro.2022.133893.

Kanagasundaram, K. and Solaiyan, E. (2023), "Smart cement-sensor composite: The evolution of nanomaterial in developing sensor for structural integrity", *Struct. Concr.*, **24**(5), 1-41. https://doi.org/10.1002/suco.202201145.

Khalid, A., Khushnood, R.A. and Ali Memon, S. (2022),

"Pyrolysis as an alternate to open burning of crop residue and scrap tires: Greenhouse emissions assessment and mechanical performance investigation in concrete", *J. Clean. Prod.*, **365**. https://doi.org/10.1016/j.jclepro.2022.132688.

Kok, M.V. and Özgür, E. (2013), "Thermal analysis and kinetics of biomass samples", *Fuel Proc. Technol.*, **106**, 739-743. https://doi.org/10.1016/j.fuproc.2012.10.010.

Li, C., Fan, Z., Wu, S., Li, Y., Gan, Y. and Zhang, A. (2018), "Effect of carbon black nanoparticles from the pyrolysis of discarded tires on the performance of asphalt and its mixtures", *Appl. Sci.*, **8**(4), 1-16. https://doi.org/10.3390/app8040624.

Lim, S. and Mondal, P. (2014), "Micro- and nano-scale characterization to study the thermal degradation of cement-based materials", *Mater. Charact.*, **92**, 15-25. https://doi.org/10.1016/j.matchar.2014.02.010.

Long, W.J., Xiao, B.X., Gu, Y.C. and Xing, F. (2018), "Micro- and macro-scale characterization of nano- SiO2 reinforced alkali activated slag composites", *Mater. Charact.*, **136**, 111-121. https://doi.org/10.1016/j.matchar.2017.12.013.

Ma, Y., Zhao. H., Zhang, X., Fan, C., Zhuang, T., Sun, C. and Zhao, S. (2022), "Structure optimization of pyrolysis carbon black from waste tire and its application in natural rubber composites", *Appl. Surf. Sci.*, **593**, 153389. https://doi.org/10.1016/j.apsusc.2022.153389

Mahmood, A., Khushnood, R.A. and Zeeshan, M. (2020), "Pyrolytic carbonaceous reinforcements for enhanced electro-magnetic and fracture response of cementitious composites", *J. Clean. Prod.*, **248**, 119288. https://doi.org/10.1016/j.jclepro.2019.119288.

Maroufi, S., Mayyas, M. and Sahajwalla, V. (2017), "Nano-carbons from waste tyre rubber: An insight into structure and morphology", *Waste Manag.*, **69**, 110-116. https://doi.org/10.1016/j.wasman.2017.08.020.

Martínez, J.D., Cardona-Uribe, N., Murillo, R., García, T. and López, J.M., (2019), "Carbon black recovery from waste tire pyrolysis by demineralization: Production and application in rubber compounding", *Waste Manag.*, **85**, 574-584. https://doi.org/10.1016/j.wasman.2019.01.016.

Moasas, A.M., Amin, M.N., Khan, K., Ahmad, W., Al-Hashem, M.N.A., Deifalla, A.F. and Ahmad, A. (2022), "A worldwide development in the accumulation of waste tires and its utilization in concrete as a sustainable construction material: A review", *Case Stud. Constr. Mater.*, **17**, e01677. https://doi.org/10.1016/j.cscm.2022.e01677.

Mohajerani, A., Burnett, L., Smith, J. V., Markovski, S., Rodwell, G., Rahman, M.T., Kurmus, H., Mirzababaei, M., Arulrajah, A., Horpibulsuk, S. and Maghool, F. (2020), "Recycling waste rubber tyres in construction materials and associated environmental considerations: A review", *Resour. Conserv. Recycl.*, **155**, 104679. https://doi.org/10.1016/j.resconrec.2020.104679.

Nogueira, M., Matos, I., Bernardo, M., Pinto, F., Lapa, N., Surra, E. and Fonseca, I. (2019), "Char from spent tire rubber: A potential adsorbent of remazol yellow dye", *J. Carbon Res.*, **5**(4), 76. https://doi.org/10.3390/c5040076.

Owens, D.K. and Wendt, R.C. (1969), "Estimation of the surface free energy of polymers", *J. Appl. Polym. Sci.*, **13**, 1741-1747. https://doi.org/https://doi.org/10.1002/app.1969.070130815.

Papanikolaou, I., Ribeiro de Souza, L., Litina, C. and Al-Tabbaa, A. (2021), "Investigation of the dispersion of multi-layer graphene nanoplatelets in cement composites using different superplasticizer treatments", *Constr. Build. Mater.*, **293**, 123543. https://doi.org/10.1016/j.conbuildmat.2021.123543.

Parthasarathy, P., Choi, H.S., Park, H.C., Hwang, J.G., Yoo, H.S., Lee, B.K. and Upadhyay, M. (2016), "Influence of process conditions on product yield of waste tyre pyrolysis- A review", *Korean J. Chem. Eng.*, **33**(8), 2268-2286. https://doi.org/10.1007/s11814-016-0126-2.

Paul, S., Rahaman, M., Ghosh, S.K., Katheria, A., Das, T.K., Patel, S. and Das, N.C. (2023), "Recycling of waste tire by pyrolysis to recover carbon black: an alternative reinforcing filler", *J. Mater. Cycles Waste Manag.*, **25**, 1470-1481. https://doi.org/10.1007/s10163-023-01635-6.

Rai, R.S. and Bajpai, V. (2023), "One-step microwave synthesis of surface functionalized carbon fiber fabric by ZnO nano-structures", *Adv. Nano Res.*, **14**(6), 557-573. https://doi.org/10.12989/anr.2023.14.6.557

Rbihi, S., Aboulouard, A., Laallam, L. and Jouaiti, A. (2020), "Contact Angle Measurements of Cellulose based Thin Film composites: Wettability, surface free energy and surface hardness", *Surf. Interf.*, **21**, 100708. https://doi.org/10.1016/j.surfin.2020.100708.

Rosa, P. de F., Cirqueira, S.S.R., Aguiar, M.L. and Bernardo, A. (2014), "Solvothermal synthesis and characterization of silver nanoparticles", *Adv. Nano Res.*, **802**(3), 135-139. https://doi.org/10.4028/www.scientific.net/MSF.802.135

Ryms, M., Januszewicz, K., Kazimierski, P., Łuczak, J., Klugmann-Radziemska, E. and Lewandowski, W.M. (2020), "Post-pyrolytic carbon as a phase change materials (PCMs) carrier for application in building materials", *Materials*, **13**(6), 1268. https://doi.org/10.3390/ma13061268

Ryms, M., Januszewicz, K., Haustein, E., Kazimierski, P. and Lewandowski, W.M. (2022), "Thermal properties of a cement composite containing phase change materials (PCMs) with post-pyrolytic char obtained from spent tyres as a carrier", *Energy*, **239**, 121936. https://doi.org/10.1016/j.energy.2021.121936.

Sardar, H., Khushnood, R.A., Khaliq, W., Khan, H.A. and Saleem, M.F. (2022), "Influence of pyrolytic waste tire residue on the residual performance of high strength concrete exposed to elevated temperatures", *J. Build. Eng.*, **54**, 104657. https://doi.org/10.1016/j.jobe.2022.104657.

Shilpa, Kumar, R. and Sharma, A. (2018), "Morphologically tailored activated carbon derived from waste tires as high-performance anode for Li-ion battery", *J. Appl. Electrochem.*, **48**(1), 1-13. https://doi.org/10.1007/s10800-017-1129-3.

Singh, J., Kumar, M., Sharma, A., Pandey, G., Chae, K. and Lee, S. (2016), *Activated Carbons from Waste Tyre Pyrolysis: Application*, Intech, London, U.K.

Tauc, J., Grigorovici, R. and Vancu, A. (1966), "Optical properties and electronic structure of amorphous germanium", *Phys. Status Solidi B*, **15**(2), 627-637. https://doi.org/10.1002/pssb.19660150224.

Tauc, J. and Scott, T.A. (1967), "The optical properties of solids", *Phys. Today*, **20**(10), 105-107. https://doi.org/10.1063/1.3033945.

Torres, I.Z., Dominguez, A.S., Bueno, J.J.P., Meas, Y., Lopez, M.L.M. and Dector, A. (2021), "Analyzing corrosion rates of TiO2 nanotubes/titanium separation passive layer under surface and crystallization changes", *Adv. Nano Res.* **10**(3), 211-219. https://doi.org/10.12989/anr.2021.10.3.211

Trubetskaya, A., Kling, J., Ershag, O., Attard, T.M. and Schröder, E. (2019), "Removal of phenol and chlorine from wastewater using steam activated biomass soot and tire carbon black", *J. Hazard. Mater.* **365**, 846-56. https://doi.org/10.1016/j.jhazmat.2018.09.061

Uvarov, V. and Popov, I. (2007), "Metrological characterization of X-ray diffraction methods for determination of crystallite size in nano-scale materials", *Mater. Charact.*, **58**(10), 883-891. https://doi.org/10.1016/j.matchar.2006.09.002.

Uvarov, V. and Popov, I. (2013), "Metrological characterization of X-ray diffraction methods at different acquisition geometries for determination of crystallite size in nano-scale materials", *Mater. Charact.*, **85**, 111-123. https://doi.org/10.1016/j.matchar.2013.09.002.

Wang, H., Lu, G., Feng, S., Wen, X. and Yang, J. (2019), "Characterization of bitumen modified with pyrolytic carbon black from scrap tires", *Sustain.*, **11**(6), 1-13. https://doi.org/10.3390/su11061631.

Wang, M., Zhang, L., Li, A., Irfan, M., Du, Y. and Di, W. (2019) 'Comparative pyrolysis behaviors of tire tread and side wall from waste tire and characterization of the resulting chars', *J. Environ. Manage.*, **232**, 364-371. https://doi.org/10.1016/j.jenvman.2018.10.091.

Wang, Z., Wu, M., Chen, G., Zhang, M., Sun, T., Burra, K.G., Guo, S., Chen, Y., Yang, S., Li, Z., Lei, T. and Gupta, A.K. (2023), "Co-pyrolysis characteristics of waste tire and maize stalk using TGA, FTIR and Py-GC/MS analysis", *Fuel*, **337**, 127206. https://doi.org/10.1016/j.fuel.2022.127206.

Wu, I.F. and Liao, Y.C. (2021), "A chemical milling process to produce water-based inkjet printing ink from waste tire carbon blacks", *Waste Manag.*, **122**, 64-70. https://doi.org/10.1016/j.wasman.2020.12.041

Zhao, J., Huang, G., Guo, Y., Gupta, R., Liu, W.V. (2023), "Developing thermal insulation cement-based mortars using recycled carbon black derived from scrapped off-the-road tires", *Constr. Build. Mater.*, **393**, 132043. https://doi.org/10.1016/j.conbuildmat.2023.132043

CC